STRUCTURAL BIOLOGY

Structural insights into the EGO-TC–mediated membrane tethering of the TORC1-regulatory Rag GTPases

Tianlong Zhang[1]*, Marie-Pierre Péli-Gulli[2]*, Zhen Zhang[1,3], Xin Tang[1,3], Jie Ye[1], Claudio De Virgilio[2†‡], Jianping Ding[1,3†‡]

The Rag/Gtr GTPases serve as a central module in the nutrient-sensing signaling network upstream of TORC1. In yeast, the anchoring of Gtr1-Gtr2 to membranes depends on the Ego1-Ego2-Ego3 ternary complex (EGO-TC), resulting in an EGO-TC-Gtr1-Gtr2 complex (EGOC). EGO-TC and human Ragulator share no obvious sequence similarities and also differ in their composition with respect to the number of known subunits, which raises the question of how the EGO-TC fulfills its function in recruiting Gtr1-Gtr2. Here, we report the structure of EGOC, in which Ego1 wraps around Ego2, Ego3, and Gtr1-Gtr2. In addition, Ego3 interacts with Gtr1-Gtr2 to stabilize the complex. The functional roles of key residues involved in the assembly are validated by in vivo assays. Our structural and functional data combined demonstrate that EGOC and Ragulator-Rag complex are structurally conserved and that EGO-TC is essential and sufficient to recruit Gtr1-Gtr2 to membranes to ensure appropriate TORC1 signaling.

INTRODUCTION

The target of rapamycin complex 1 (TORC1) is a highly conserved protein kinase complex that acts as a central controller of cell growth, metabolism, proliferation, and differentiation in response to environmental cues (*1*). Among the various input signals, amino acids are potent activators that promote multiple anabolic responses including ribosome and protein synthesis (*2*). In mammals, the Rag guanosine triphosphatases (GTPases) are essential mediators of amino acid signaling to mammalian TORC1 (mTORC1). The Rag GTPase family consists of RagA, RagB, RagC, and RagD, with each one composed of an N-terminal GTPase domain (NTD) and a C-terminal Roadblock/LC7 domain (CTD) (*3*, *4*). RagA or RagB forms an obligate heterodimer with RagC or RagD through their respective CTDs (*5*). The nucleotide loading states of Rag GTPases determine their functions. In the presence of amino acids, RagA/B is in the guanosine 5′-triphosphate (GTP)–bound state and RagC/D in the guanosine diphosphate (GDP)–bound state. The resulting Rag heterodimer is active and capable of binding mTORC1 to promote its recruitment to lysosomal membranes, where it is in a position to interact with the small GTPase Rheb that promotes its kinase activity. When amino acids are limited, the GTP- and GDP-loading states within these Rag GTPases are inversed. The resulting Rag heterodimer is then inactive and favors the inactivation of mTORC1 (*3*, *6*). Because of the lack of a membrane-tethering motif, the Rag GTPases are recruited to lysosomes via the scaffold Ragulator/LAMTOR complex, which consists of the lysosomal membrane anchor p18/LAMTOR1 and two Roadblock domain-containing heterodimers of p14-MP1/LAMTOR2-LAMTOR3 and C7orf59-HBXIP/LAMTOR4-LAMTOR5 (*7*–*12*). In the crystal structure of the Ragulator–Rag GTPase CTD complex, p18 wraps around p14-MP1, C7orf59-HBXIP, and the dimeric CTDs of the Rag GTPases to assemble the entire complex (*8*, *11*).

In yeast, Gtr1 and Gtr2 are orthologs of mammalian Rag GTPases, which also form a functional obligate heterodimer (*5*, *13*). Similar to Rag GTPases in higher eukaryotes, Gtr1 and Gtr2 are in their GTP- and GDP-bound states, respectively, when nutrients are plentiful (*14*). The activity of the Gtr1-Gtr2 module is regulated by the Gtr1 GTPase activating protein (GAP) complex SEACIT (SEA subcomplex inhibiting TORC1) and its upstream regulator SEACAT (SEA subcomplex activating TORC1), the heterodimeric Gtr2 GAP complex Lst4-Lst7, the Gtr1 guanine nucleotide exchange factor (GEF) Vam6, and the leucyl–transfer RNA synthetase (*14*–*16*). Analogous to mammalian Ragulator, the yeast Ego1-Ego2-Ego3 ternary complex (EGO-TC) interacts with Gtr1-Gtr2 to form a pentameric EGO complex (EGOC) (*17*, *18*). Ego1 is equivalent to p18, which anchors the EGOC to the vacuolar and endosomal membranes through N-terminal lipid modifications, whereas Ego2 and Ego3 are equivalent to C7orf59/HBXIP and p14/MP1, respectively. The EGOC assembles at the surfaces of vacuoles and perivacuolar endosomes and regulates spatially distinct pools of TORC1, which phosphorylate functionally divergent effectors such as vacuolar Sch9 and endosomal Atg13 and Vps27 (*19*). Cells that lack any component of the EGOC fail to recover from a rapamycin-induced growth arrest and show impaired TORC1 activity (*14*, *18*). Overexpression of $Gtr1^{GDP}$ inhibits TORC1 and induces autophagy even under nutrient-rich conditions (*14*, *19*, *20*), which indicates that the EGOC can control TORC1 both positively and negatively.

Previously, we determined the crystal structure of the EGO-TC showing that Ego1 interacts with Ego3 via its C-terminal tail and that this interaction is further stabilized by Ego2 through its association with the C-terminal α4 helix of Ego1 (*18*). However, the EGO-TC contains fewer components than the pentameric Ragulator. Thus far, it remains unclear how the EGO-TC fulfills its Gtr1-Gtr2 membrane-recruiting function and whether this involves additional yet unidentified component(s). Here, we report the crystal structure of the EGO-TC in complex with full-length Gtr1-Gtr2. We show that the EGO-TC is sufficient to interact with Gtr1-Gtr2 to form a stable and functional EGOC. The key residues involved in the assembly of the complex are validated with functional assays. The structural and functional data together provide

[1]State Key Laboratory of Molecular Biology, CAS Center for Excellence in Molecular Cell Science, Institute of Biochemistry and Cell Biology, Shanghai Institutes for Biological Sciences, University of Chinese Academy of Sciences, Chinese Academy of Sciences, 320 Yue-Yang Road, Shanghai 200031, China. [2]Department of Biology, University of Fribourg, CH-1700 Fribourg, Switzerland. [3]School of Life Science and Technology, ShanghaiTech University, 393 Hua-Xia Zhong Road, Shanghai 201210, China.
*These authors contributed equally to this work.
†These authors jointly supervised this work.
‡Corresponding author. Email: claudio.devirgilio@unifr.ch (C.D.V.); jpding@sibcb.ac.cn (J.D.)

the molecular basis for the EGO-TC functioning as a scaffold in the membrane anchorage of Gtr1-Gtr2 and the subsequent TORC1 regulation.

RESULTS

Overall structure of the EGOC

To facilitate crystal growth, the N-terminal myristoylation and palmitoylation region of Ego1 (residues 1 to 32) was truncated. Residues 98 to 121 exhibit a high variability among different yeast species (fig. S1). The deletion of these residues (98 to 121) in Ego1 did neither cause any substantial changes in the vacuolar localization of Ego1 itself (fig. S2A) nor in the assembly of the EGOC and its capacity to promote TORC1 activity (figs. S2, B and C, and S3, A and B). This set of residues was therefore also deleted in recombinant Ego1, which was coexpressed with full-length Ego2, Ego3, Gtr1, and Gtr2. In the purified pentameric EGOC, both Gtr1 and Gtr2 were loaded with GppNHp, a nonhydrolyzable GTP analog. The structure of the EGOC was solved by the molecular replacement (MR) method using the previously solved EGO-TC and Gtr1-Gtr2 structures as the searching models, and each asymmetric unit contains two EGOC molecules (fig. S4). In molecule A, most residues of all components in the complex are well defined; however, in molecule B, the GTPase domain of Gtr2 is largely disordered probably because of fewer crystal packing contacts (fig. S4). Besides that, the two molecules are very similar with a root mean square deviation (RMSD) of 0.5 Å for 482 Cα atoms. Thus, molecule A is used for structural analysis hereafter.

The structure of the EGOC comprises an EGO-TC and a Gtr1-Gtr2 heterodimer (Fig. 1, A and B). Ego1 forms a U-shaped helical structure over the traced length (residues 43 to 95 and 140 to 184) including helices α1 to α4, while the N-terminal region of residues 33 to 42 and the middle region of residues 97 to 138 [encompassing the deleted segment (residues 98 to 121) in the construct] are not defined in the electron map (fig. S5). From the N-terminal α1 helix to the C-terminal tail, Ego1 interacts sequentially with the other four components Gtr2, Ego3, Ego2, and Gtr1. Ego2 exhibits an incomplete Roadblock domain fold of ββαβββ, which is similar to the Ragulator components C7orf59 and HBXIP (ββαβββα) but lacks a C-terminal α helix. Ego3 adopts a unique Roadblock domain fold of αββββαββββα, which contains an extra β hairpin (β1 and β2) and a β strand (β5) compared with the Ragulator components p14 and MP1 (αββαββββα). Gtr1 and Gtr2 form a heterodimer via their CTDs with a pseudo-twofold symmetry, and both NTDs are bound with a GppNHp and a Mg^{2+}, which are very well defined in the electron density map (fig. S5A). The overall conformation of the $Gtr1^{GppNHp}$-$Gtr2^{GppNHp}$ heterodimer in the EGOC is very similar to that of the $Gtr1^{GppNHp}$-$Gtr2^{GppNHp}$ heterodimer in the free form [Protein Data Bank (PDB) code 3R7W] with an RMSD of 1.3 Å for 560 aligned Cα atoms, suggesting that the binding of the EGO-TC induces no notable conformational change of Gtr1-Gtr2 (fig. S6A). Consistent with the previous finding (*13*), the segment covering residues 28 to 70 in the GTPase domain of $Gtr2^{GppNHp}$ exhibits a conformational rearrangement compared with the most active form of the

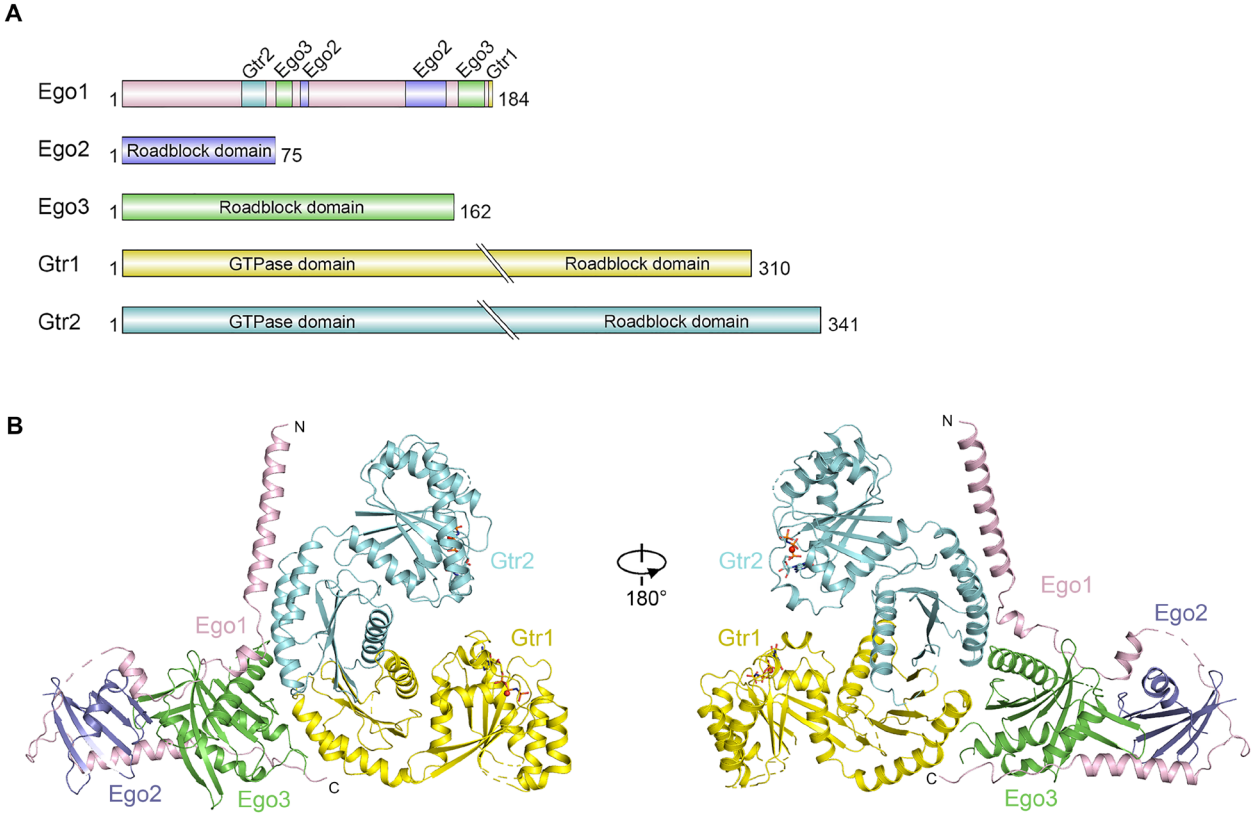

Fig. 1. Crystal structure of the EGOC. (**A**) Schematic diagram of the EGOC components. The interacting regions of Ego1 with Ego2, Ego3, Gtr1, and Gtr2 are indicated. The Roadblock domains and GTPase domains in Ego2, Ego3, Gtr1, and Gtr2 are also indicated. (**B**) Overall structure of the EGOC in two different views with Ego1 shown in pink, Ego2 in blue, Ego3 in green, Gtr1 in yellow, and Gtr2 in cyan.

$Gtr1^{GTP}$-$Gtr2^{GDP}$ heterodimer (PDB code 4ARZ) induced by the GTP-to-GDP conversion (fig. S6B), while the Roadblock domains of Gtr1 and Gtr2 do not undergo a notable conformational change (fig. S6C).

Assembly of the EGO-TC

In the previously determined EGO-TC structure, the N-terminal region of Ego1 was degraded during crystallization, and only the C-terminal region (residues 146 to 184) was observed, which forms a long α4 helix flanked by two loops (*18*). In the current EGOC structure, the previously unobserved N-terminal region of Ego1 forms a long (α1) and two short α helices (α2 and α3), which wrap around Ego2 and Ego3 and play an important role in the assembly of the EGO-TC (Fig. 1B). Specifically, the α2 helix and the following loop flank on one side of and make extensive interactions with Ego3 (Fig. 2A). The side chains of the strictly conserved Ile^{77}, Ile^{82}, and Val^{83} of Ego1 stack on the hydrophobic surface of helix α2 and strand β6 of Ego3 and make hydrophobic interactions with the side chains of Leu^{74}, Leu^{75}, Ile^{76}, Tyr^{110}, and Met^{112} of Ego3; and the side chain of Gln^{85} of Ego1 forms a hydrogen bond with the side chain of Asp^{83} of Ego3. Afterward, the α3 helix of Ego1 makes a ~90° turn and packs along the one-helix side of Ego2, and the following region

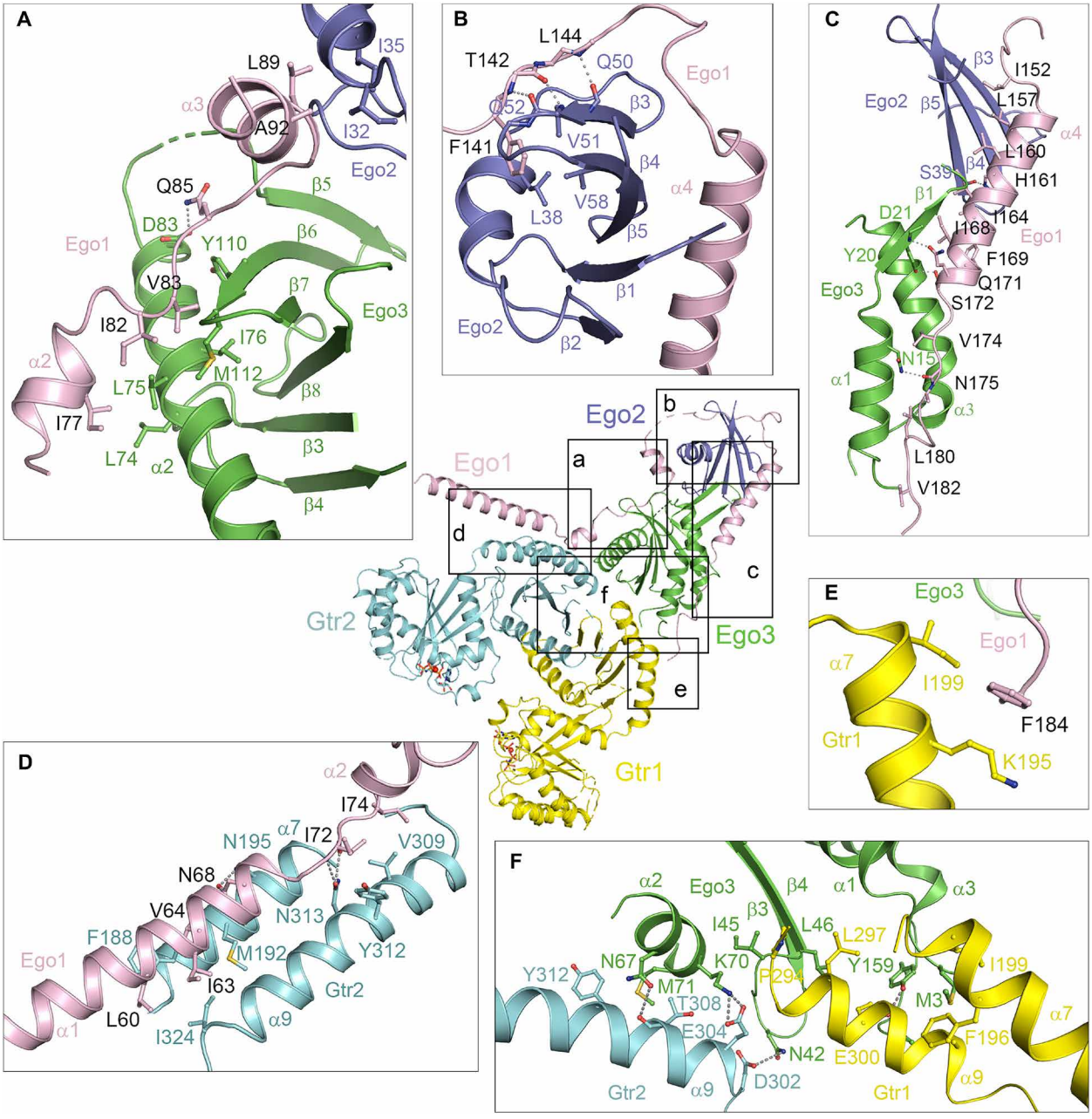

Fig. 2. Detailed interactions among different EGOC components. Close-up view of Ego1 interacting with Ego2 and Ego3 (**A** to **C**), with Gtr2 (**D**), and with Gtr1 (**E**). (**F**) Detailed interactions of Ego3 with Gtr1-Gtr2. The residues involved in the interactions are shown in ball-and-stick models and colored as in Fig. 1B. For clarity, the residues of Ego1 are marked in black. The hydrophilic interactions are indicated with dashed lines.

(residues 97 to 138) extends to the solvent area and becomes disordered (Fig. 2A). At this interface, Ego1 has only minor interactions with Ego2: The side chains of Leu^{89} and Ala^{92} make hydrophobic interactions with the side chains of Ile^{32} and Ile^{35} of Ego2. Moreover, the loop following the disordered region of Ego1 folds along the edge of the β sheet (β3) of Ego2 (Fig. 2B). This interface is mostly stabilized by three hydrogen bonds between the main chains of Thr^{142} and Leu^{144} of Ego1 and the main chains of Gln^{50} and Gln^{52} of Ego2. In addition, the side chain of Phe^{141} of Ego1 also makes hydrophobic interactions with the side chains of Leu^{38}, Val^{51}, and Val^{58} of Ego2.

Furthermore, the C-terminal α4 helix and the following loop of Ego1 flank on the other side of Ego2 and Ego3 in a similar manner to the one observed in the previously determined EGO-TC structure (Fig. 2C). Briefly, the N-terminal part of helix α4 of Ego1 lies on the top of the β sheet of Ego2, the C-terminal part of helix α4 lies on the top of the β1-β2 hairpin and the α3 helix of Ego3, and the C-terminal tail of Ego1 inserts into the α1 and α3 helices of Ego3. This interface involves extensive hydrophilic and hydrophobic interactions and is essential for the assembly of the EGO-TC as deletion of helix α4, and the following loop of Ego1 disrupted its interactions with both Ego2 and Ego3 and abolished the vacuolar localization of Ego2, Ego3, Gtr1, and Gtr2 (*18*). Together, the U-shaped Ego1 wraps around the Ego2 and Ego3 from both sides to form a stable and functional EGO-TC.

Interactions between the EGO-TC and Gtr1-Gtr2

In the EGOC structure, the EGO-TC interacts with the CTDs of both Gtr1 and Gtr2 via Ego1 and Ego3 (Figs. 1 and 2). Specifically, the N-terminal α1 helix of Ego1 forms a three-helix bundle with two α helices (α7 and α9) of the Gtr2 CTD (Fig. 2D). A series of hydrophobic residues including Leu^{60}, Ile^{63}, and Val^{64} of Ego1 pack against hydrophobic residues Phe^{188}, Met^{192}, and Ile^{324} of Gtr2 to stabilize the helix bundle. In addition, the side chain of Asn^{68} at the C-terminal end of helix α1 forms a hydrogen bond with the side chain of Asn^{195} of Gtr2. Thereafter, the α1-α2 connecting loop of Ego1 protrudes into the two α helices of the Gtr2 CTD: The side chains of Ile^{72} and Ile^{74} of Ego1 make hydrophobic interactions with Val^{309} and Tyr^{312} of Gtr2; in addition, the main chain of Ile^{72} forms two hydrogen bonds with the side chain of Asn^{313} of Gtr2. After wrapping around Ego3 and Ego2, the C-terminal tail of Ego1 makes a minor interaction with the Gtr1 CTD: The extreme C-terminal residue Phe^{184} of Ego1 forms hydrophobic interactions with the side chains of Lys^{195} and Ile^{199} of Gtr1 (Fig. 2E). However, Phe^{184} of Ego1 is not conserved in other yeast species (fig. S1), which might suggest that the interaction interface between Ego1 and Gtr1 is less critical in the EGOC assembly.

Besides Ego1, Ego3 also makes extensive hydrophobic and hydrophilic interactions with the CTDs of both Gtr1 and Gtr2 via the α2 helix, the β3-β4 loop, and the N-terminal and C-terminal tails (Fig. 2F). Specifically, the α2 helix of Ego3 interacts with the α9 helix of the Gtr2 CTD. The side chain of Asn^{67} of Ego3 forms a hydrogen bond with the main chain of Thr^{308} of Gtr2; the side chain of Lys^{70} of Ego3 forms a salt bridge with the side chain of Glu^{304} of Gtr2; and Met^{71} of Ego3 makes hydrophobic contacts with Thr^{308} and Tyr^{312} of Gtr2. The β3-β4 loop of Ego3 protrudes into a gap between the two α9 helices of the Gtr1 and Gtr2 CTDs. The side chain of Asn^{42} of Ego3 forms a hydrogen bond with the side chain of Asp^{302} of Gtr2, and Ile^{45} and Leu^{46} of Ego3 make hydrophobic contacts with Pro^{294} and Leu^{297} of Gtr1. In addition, the side chain of Met^{3} on the N-terminal tail of Ego3 makes hydrophobic contacts with Phe^{196} and Ile^{199} of Gtr1; the side chain of Tyr^{159} on the C-terminal tail of Ego3 forms a hydrogen bond with the side chain of Glu^{300} of Gtr1.

Functional validation of the interacting residues on Ego1 and Ego3

To confirm the functional role of the structurally identified contact sites in the in vivo assembly of the EGOC, we generated several Ego1 and Ego3 mutants and analyzed their respective subcellular distribution along with their capacity to interact with the Gtrs and to promote TORC1 activity. First, we examined the interaction interface between the N-terminal region of Ego1 and Gtr2 (Fig. 3, A to C). All the tested Ego1 variants (i.e., $Ego1^{L53D/L54D}$, $Ego1^{I63D/V64D}$, and $Ego1^{I72D/I74D}$) concentrated on vacuolar and perivacuolar/endosomal membranes like $Ego1^{WT}$ (Fig. 3A). Consistent with the assumption that the Leu^{53} and Leu^{54} residues play no role in Ego1 binding to Gtr2, no changes in Gtr2 localization were observed in cells expressing $Ego1^{L53D/L54D}$. By contrast, and as anticipated, expression of the $Ego1^{I63D/V64D}$ or $Ego1^{I72D/I74D}$ allele abolished completely the vacuolar recruitment of Gtr2 (Fig. 3B). Loss of Gtr2 association with these latter Ego1variants was further corroborated by coimmunoprecipitation (co-IP) analysis (Fig. 3C).

Second, we examined the interaction interface between the C-terminal region of Ego1 and Gtr1 (Fig. 3, D and E). As Ego1 has very minor interactions with Gtr1, it is not surprising to observe that the $Ego1^{F184A}$ allele, which itself localized normally to and ensured proper localization of Gtr1 at the vacuolar membrane (Fig. 3, A and D), interacted normally with Gtr1 in co-IP analyses (Fig. 3E). Last, we inspected the interaction interface between Ego3 and Gtr1 (Fig. 3, F to H). Previously, we found that the quadruple Ego3 mutant (N67A/N68A/K70A/M71A) could not interact with Gtr1-Gtr2 (*21*), which is consistent with the interactions between Ego3 and Gtr2. The single $Ego3^{M71D}$ allele, which properly localized at vacuolar membranes (Fig. 3F), was also unable to promote the association of the Gtr1-Gtr2 module to the vacuolar membrane (Fig. 3G). In addition, in accordance with the expectations from our structural data, we found that the $Ego3^{M3D}$ allele, which normally localized at the vacuolar membrane (Fig. 3F), failed to interact with and recruit Gtr1 to the vacuolar membrane (Fig. 3, G and H). All the Ego1 and Ego3 variants that failed to bind the Gtrs, and hence to assemble the EGOC, exhibited rapamycin sensitivity and reduced TORC1 activity (fig. S3, A to D). Taken the structural and functional data together, we conclude that the interactions of Ego1 with Gtr2 and those of Ego3 with Gtr1-Gtr2 are essential for the assembly of the EGOC, whereas the interactions of Ego1 with Gtr1 are not.

DISCUSSION

The Rag/Gtr GTPases form a heterodimeric complex, which serves as a central element of the nutrient-sensing signaling network upstream of TORC1 both in yeast and in mammals (*22*). Unlike other lipid modified small GTPases such as Ras and Rabs, their anchoring to the membranes depends on specific scaffolds. In budding yeast, the vacuolar EGO-TC, which consists of Ego1, Ego2, and Ego3, acts as a scaffold that associates with the vacuolar surface via the N-terminal palmitoyl- and myristoyl- moieties of Ego1 and then recruits the Gtr1-Gtr2 heterodimer (*14*, *18*, *21*). In this work, we determined the crystal structure of the EGO-TC in complex with full-length Gtr1-Gtr2 and showed that, in the EGOC structure, the

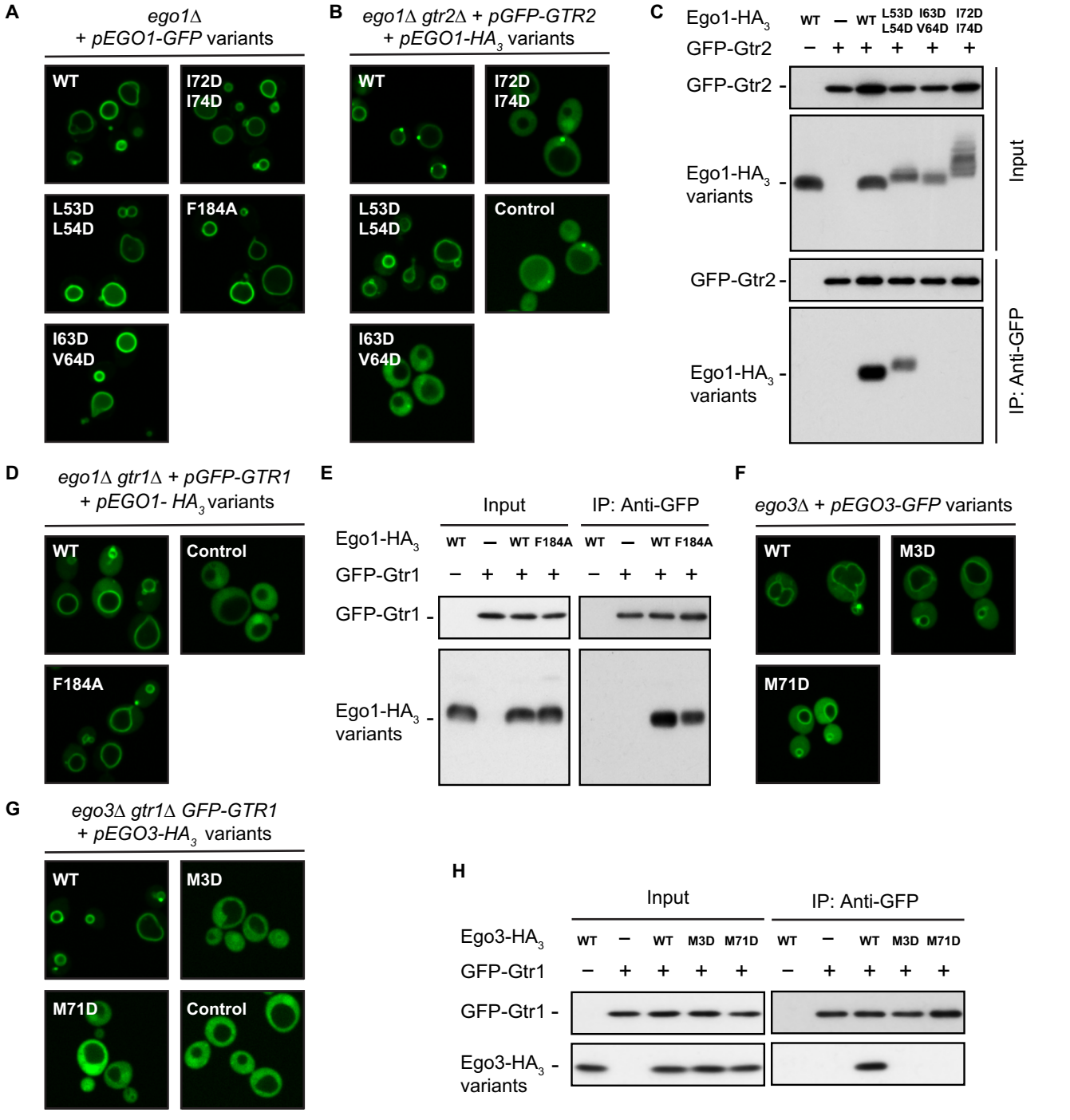

Fig. 3. Subcellular localization and Gtr-association of Ego1 and Ego3 variants mutated on key structurally predicted interacting residues. (**A**) Localization of indicated Ego1-GFP (green fluorescent protein) alleles was examined in prototrophic *ego1*Δ cells grown exponentially in synthetic drop-out medium. (**B**) Localization of GFP-Gtr2 was assessed in prototrophic *ego1*Δ *gtr2*Δ cells coexpressing, or not (Control), indicated Ego1-HA_3 variants, and cultured as in (A). (**C**) Anti-GFP immunoprecipitations (IPs) were carried out on lysates from cells described in (B) or from *ego1*Δ cells expressing $Ego1^{WT}$-HA_3. Input and IP fractions were analyzed by Western blot and probed with anti-HA and anti-GFP antibodies. (**D**) Localization of GFP-Gtr1 was examined in prototrophic *ego1*Δ *gtr1*Δ cells coexpressing, or not (Control), either $Ego1^{WT}$-HA_3 or $Ego1^{F184A}$-HA_3, and cultured as in (A). (**E**) Anti-GFP IPs were carried out on lysates from cells described in (D) or from *ego1*Δ cells expressing $Ego1^{WT}$-HA_3, and processed as in (C). (**F**) Localization of $Ego3^{WT}$-GFP or indicated Ego3-GFP alleles was examined in prototrophic *ego3*Δ cells grown as in (A). (**G**) Localization of genomically integrated GFP-Gtr1 was assessed in prototrophic *ego3*Δ *gtr1*Δ cells coexpressing, or not (Control), either $Ego3^{WT}$-HA_3 or the indicated Ego3-HA_3 mutants, and cultured as in (A). (**H**) Anti-GFP IPs were performed on lysates from cells described in (G) or from *ego3*Δ cells expressing $Ego3^{WT}$-HA_3, and processed as in (C). HA, human influenza hemagglutinin.

rope-like Ego1 wraps around and sequentially ties the other four Roadblock domain-containing components Gtr2, Ego3, Ego2, and Gtr1 together. The EGO-TC and Gtr1-Gtr2 interaction interface is predominantly dictated by hydrophobic interactions between the N-terminal α1 helix of Ego1 and the Gtr2 CTD (Fig. 2, A to E). Ego3 also contributes a critical interaction interface with the CTDs of both Gtr1 and Gtr2 (Fig. 2F). Disruption of the interface of either Ego1 or Ego3 with Gtr1-Gtr2 impairs the vacuolar recruitment of Gtr1-Gtr2 (Fig. 3, B to G). Among the EGO-TC components, Ego2 has no direct interaction with Gtr1-Gtr2 but plays a critical role in the assembly of the EGO-TC and hence in the formation of the EGOC. Compared with the free $Gtr1^{GTP}$-$Gtr2^{GDP}$ structure, the CTDs of Gtr1 and Gtr2 do not display a notable conformational change and most of the residues involved in the interactions with EGO-TC are in comparable positions (fig. S6C). Therefore, EGO-TC may interact with $Gtr1^{GTP}$-$Gtr2^{GDP}$ in a similar manner as with $Gtr1^{GppNHp}$-$Gtr2^{GppNHp}$.

Yeast Gtr1 and Gtr2 are homologs of mammalian RagA/B and RagC/D, respectively, and the EGO-TC is considered as the functional counterpart of the mammalian Ragulator complex despite low sequence identities (*18*). Comparison of the structures of the EGOC and the Ragulator-RagA(CTD)-RagC(CTD) complex reveals a high degree of similarity in the overall architecture, indicating that the EGOC and the Ragulator-Rag complex are structurally conserved (Fig. 4 and fig. S7A). Particularly, the Roadblock domains of Gtr1-Gtr2 can be well superimposed onto those of RagA-RagC; Ego1, Ego2, and Ego3 overlap spatially with p18, HBXIP, and p14, respectively. Both Ego1 and p18 consist of four α helices, and the N-terminal α1 helix of both Ego1 and p18 plays a crucial role in the interactions with the Gtr/Rag GTPases. In addition, the key residues of the α1 helix of Ego1 and p18 that participate in the interactions with the Gtr/Rag GTPases are highly similar (Fig. 2D and fig. S7B). Moreover, the binding modes between Ego3 and Gtr1-Gtr2 and between p14 and RagA-RagC are also very similar. Particularly, the α2 helix and the β3-β4 loop of both Ego3 and p14 pack on the four-helix side of the Gtr/Rag CTDs, and both the N- and C-terminal tails of Ego3 and p14 are involved in the interactions with Gtr1/RagA. In addition, several residues of Ego3 and p14 at the interaction interfaces are conserved, especially for Ile^{45} and Leu^{46} of Ego3 and Leu^{31} and Leu^{32} of p14 in the protruding β3-β4 loop (Fig. 2F and fig. S7C). Nonetheless, the structural comparison also reveals some substantial differences. Notably, the C-terminal tail of p18 contributes an essential interface with RagA (*11*), whereas the C-terminal tail of Ego1 is much shorter and makes only minor interactions with Gtr1 (Figs. 2E and 4). The other obvious difference is that the EGO-TC consists of three components, while the Ragulator complex comprises two additional components: MP1 and C7orf59 (Fig. 4). In the EGO-TC, Ego1 wraps across the β strands of Ego2 and Ego3, thereby impeding the binding of additional components to form typical Roadblock heterodimers like the MP1-p14 and C7orf59-HBXIP heterodimers (Fig. 2, A and B). The involvement of a higher number of Roadblock domain containing components within the Ragulator complex may account for the requirement to fulfill more complicated/elaborated functions in higher eukaryotes.

In addition to functioning as a scaffold for recruiting the Rag GTPases, the Ragulator was also shown to have a GEF activity toward RagA/B through a noncanonical mechanism together with the lysosomal arginine sensor SLC38A9 (*12*, *23*). To exert the GEF activity, the Ragulator resolves the inactivated state of $RagA^{GDP}$-$RagC^{GTP}$ by triggering nucleotide release from RagC, thereby forming a $RagA^{GDP}$-$RagC^{GDP}$ heterodimer. Upon activation by arginine, SLC38A9 then converts RagA from the GDP- to the GTP-bound state, hence yielding the activated $RagA^{GTP}$-$RagC^{GDP}$ heterodimer (*23*). Because of the absence of the GTPase domains in the reported structures of the

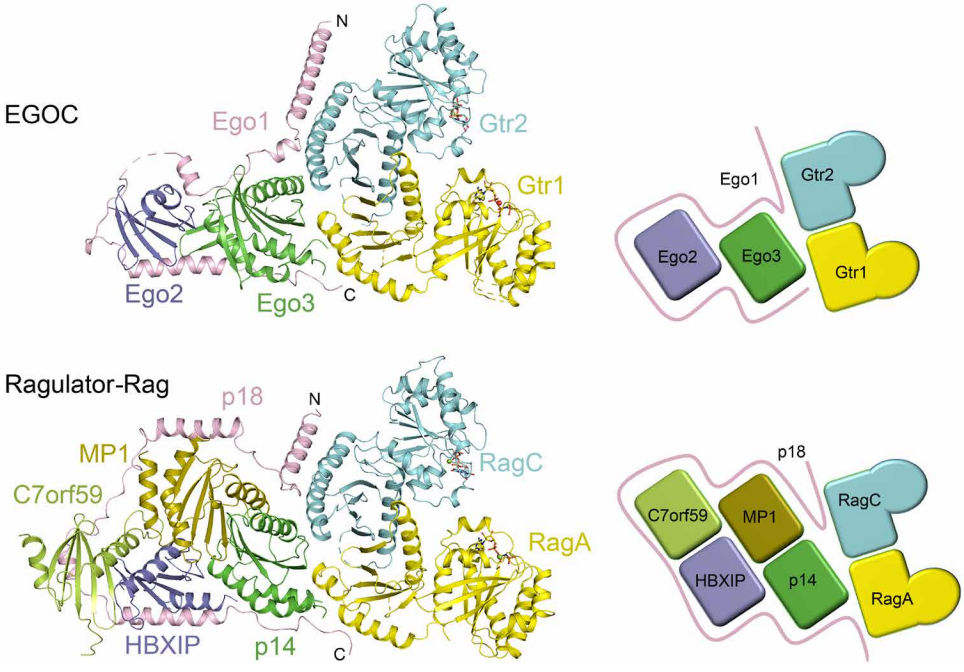

Fig. 4. Structural comparison of the EGOC and the Ragulator-Rag complex. The structure of the Ragulator-Rag complex containing both GTPase and Roadblock domains of RagA-RagC are modeled from the Ragulator-RagA(CTD)-RagC(CTD) complex (PDB code 6EHR) and the Gtr1-Gtr2 heterodimer (PDB code 3R7W). Cartoon representations of the EGOC and the Ragulator-Rag complex are shown on the right side.

Ragulator-RagA(CTD)-RagC(CTD) complex (*8*, *11*), the detailed mechanism by which the Ragulator exerts the GEF function remains elusive. However, in the EGOC structure, the EGO-TC interacts exclusively with the Roadblock domains and not with the GTPase domains of Gtr1-Gtr2 (Fig. 1). Furthermore, comparison of the free Gtr1-Gtr2 heterodimer and the EGOC structures reveals no notable conformational changes in the nucleotide-binding pocket and the switch regions of both Gtr1 and Gtr2 upon formation of the EGOC (fig. S6A). Therefore, the EGO-TC very likely lacks a GEF activity toward Gtr1 or Gtr2 in an either canonical or noncanonical manner.

Table 1. Summary of diffraction data collection and structure refinement statistics. Numbers in parentheses refer to the highest resolution shell.

Diffraction data	
Wavelength (Å)	0.9789
Space group	$P2_12_12_1$
Cell parameters	
a, *b*, *c* (Å)	81.68, 120.55, 323.27
Resolution (Å)	49.2–3.20 (3.38–3.20)
Observed reflections	283,819 (16,435)
Unique reflections ($I/\sigma(I) > 0$)	36,895 (1853)
Average redundancy	7.7 (8.9)
Average $I/\sigma(I)$	10.6 (1.4)
Spherical completeness (%)	68.9 (22.8)
Ellipsoidal completeness (%)	94.1 (83.3)
R_{merge}*	17.3 (167.9)
$CC_{1/2}$	0.997 (0.461)
Refinement and structure model	
Reflections ($Fo \geq 0\sigma(Fo)$)	
Working set	33,165
Test set	1863
R_{work}/R_{free} (%)†	23.0/28.5
No. of protein atoms	13,043
No. of ligand/ion atoms	99
Average B factor (Å^2)	
All atoms	72.0
Protein	72.0
GppNHp	73.3
Mg	67.7
RMSD	
Bond lengths (Å)	0.007
Bond angles (°)	1.20
Ramachandran plot (%)	
Favored	93.4
Allowed	6.6
Disallowed	0.0

*$R_{merge} = \Sigma_{hkl}\Sigma_i|I_i(hkl)_i - \langle I(hkl)\rangle|/\Sigma_{hkl}\Sigma_i I_i(hkl)$. †*R*-factor $= ||F_o|-|F_c||/|F_o|$.

Instead, other elements such as Vam6 or associated proteins may function as a GEF for Gtr1 in budding yeast (*14*).

In response to amino acids, the Ragulator–Rag GTPase complex is thought to directly interact with Raptor in mTORC1 to promote the translocation of mTORC1 to the lysosomal membrane where the TORC1 activator Rheb is localized (*3*). Similar to the Ragulator–Rag GTPase complex, the EGOC interacts with the yeast TORC1 subunit Kog1 or Tco89 to promote the activity of TORC1 in yeast (*24*). However, the cellular location of yeast TORC1 at the vacuolar membrane and within perivacuolar/endosomal foci does not depend on the presence of amino acids (or nitrogen) (*14*, *17*, *19*). Therefore, the EGOC seems not to function as an anchoring platform for TORC1 to vacuolar and endosomal membranes. Instead, the vacuolar and perivacuolar endosomal EGOC regulates spatially distinct pools of TORC1 (*19*), suggesting that EGOC functions as a signaling platform to mediate signals to TORC1. Exposure of the GTPase domains of Gtr1 and Gtr2 to the surface of the EGOC may facilitate binding of downstream effectors whose identity has not yet been elucidated.

MATERIALS AND METHODS

Plasmid construction and protein purification

The DNA fragments encoding *EGO1*, *EGO2*, and *EGO3* were amplified by polymerase chain reaction from the *Saccharomyces cerevisiae* complementary DNA (cDNA) library. The *EGO1* mutant containing deletion of residues 1 to 32 and 98 to 121 (Δ1-32 and Δ98-121) was cloned into the pACYCDuet-1 vector (Novagen). Wild-type *EGO2* and *EGO3* were cloned into the cloning sites I and II of the pRSFDuet-1 vector (Novagen), respectively. The construct of *GTR1-GTR2* was provided by Y. Xu (Fudan University, Shanghai, China), in which the cDNAs of full-length *GTR1* and *GTR2* were cloned into the cloning sites I and II of a modified pETDuet-1 vector (Novagen), respectively, attached with an N-terminal His_6 tag and a TEV (tobacco etch virus) protease cleavage site upstream the *GTR1* coding region. All components of the EGOC were coexpressed in *Escherichia coli* BL21 (DE3) CodonPlus strain (Tiangen), and the transformed cells were grown at 37°C in LB medium (Sangon) until optical density at 600 nm reached 0.8 and then induced with 0.2 mM isopropyl-β-D-thiogalactopyranoside for 18 hours at 16°C. Cells were harvested by centrifugation, resuspended in a lysis buffer [30 mM tris-HCl (pH 7.5), 1 mM $MgCl_2$, and 150 mM NaCl], and lysed by sonication. The EGOC was then purified by affinity chromatography using a Ni–nitrilotriacetic acid column (Qiagen), and the resulting elution was incubated with the TEV protease to remove the N-terminal His_6 tag of Gtr1. The mixture was concentrated and incubated for 1 hour at room temperature (~25°C) in the presence of 5 mM EDTA. EDTA was then removed by desalting. After supplementing with 10 mM $MgCl_2$ and 10-fold excess of GppNHp, the GppNHp-bound EGOC was separated from excessive nucleotide by gel filtration using a Superdex 200 10/60 column (preparative grade, GE Healthcare) pre-equilibrated with a storage buffer [10 mM Hepes (pH 7.5), 1 mM $MgCl_2$, 150 mM NaCl, and 1 mM dithiothreitol].

Crystallization and structure determination

Crystallization of the EGOC was performed using the hanging drop vapor diffusion method by mixing 1.5 μl of protein solution (about 10 mg/ml) and 1.5 μl of reservoir solution at 16°C. Crystals of the EGOC were obtained from drops consisting of a reservoir solution of 100 mM Hepes (pH 7.5), 200 mM NaCl, and 12% (w/v) polyethylene

glycol (molecular weight 8000). Diffraction data were collected at −175°C at BL19U1 of National Facility for Protein Science in Shanghai, China and were processed, integrated, and scaled together with XDS (x-ray detector software) (*25*). The diffraction patterns exhibit strong anisotropic characteristics. The anisotropy of the diffraction data was also revealed by the Diffraction Anisotropy Server (*26*), which recommends the resolution limits of the data to be truncated to 3.5, 4.5, and 3.2 Å along the reciprocal space directions a*, b*, and c*, respectively (fig. S8). Thus, the original unmerged diffraction data were subjected to anisotropy correction using the STARANISO server (*27*), and the resultant diffraction data were used for structure refinement. The statistics of the diffraction data are summarized in Table 1.

The structure of the EGOC was solved by the MR method implemented in Phenix (*28*) using the structures of Gtr1-Gtr2 (PDB code 3R7W) and of the EGO-TC (PDB code 4XPM) as search models. Structure refinement was carried out using Phenix and Refmac5 (*28*, *29*). Model building was performed manually using Coot (*30*). Most of the residues at the interaction interfaces between different protein components and the GppNHp molecules bound to the GTPase domains of Gtr1-Gtr2 were well defined in the electron density map (fig. S5, A to D). Structural analysis was carried out using programs in the CCP4 suite (*31*). Structure figures were generated using PyMOL (*32*). Statistics of the structure refinement and the quality of the final structure model are also summarized in Table 1.

Yeast plasmids and strains

S. cerevisiae strains used in this study are listed in table S1. Prototrophic strains were grown to exponential phase at 30°C in synthetic defined medium (0.17% yeast nitrogen base, 0.5% ammonium sulfate, and 2% glucose) complemented with the appropriate nutrients (0.2% drop-out mix) for plasmid maintenance. For rapamycin sensitivity assay, exponentially growing cultures were spotted onto rich medium [YPD (1% yeast extract, 2% peptone, and 2% dextrose)] supplemented with either vehicle (90% ethanol and 10% Tween 20) or rapamycin (5 ng/ml). Yeast plasmids used in this study are listed in table S2. All the constructs generated in this work were verified by sequencing. Unless otherwise specified, all the tagged EGOC fusion proteins were expressed from *CEN-ARS* plasmids under the control of their endogenous promoter.

Fluorescence microscopy, co-IP, and TORC1 activity measurements

For these experiments, exponentially growing cells were processed as described previously (*33*).

SUPPLEMENTARY MATERIALS

Supplementary material for this article is available at http://advances.sciencemag.org/cgi/content/full/5/9/eaax8164/DC1

Fig. S1. Sequence alignment of Ego1 from different species as analyzed by ESPript 3.0 (*34*).

Fig. S2. Deletion of residues 98 to 121 of Ego1 does not affect the vacuolar membrane location of Ego1 nor the subsequent vacuolar recruitment of the other EGOC components.

Fig. S3. Strains expressing Ego1 and Ego3 mutant variants that are unable to bind the Rag GTPases are sensitive to rapamycin and have reduced TORC1 activity.

Fig. S4. Overall structure of the two EGOC molecules in the asymmetric unit.

Fig. S5. Representative composite 2Fo-Fc omit maps (contoured at 1σ) of the EGOC (molecule A).

Fig. S6. Structural comparison of associated and free Gtr1-Gtr2 heterodimers.

Fig. S7. Structural comparison of the EGOC and the Ragulator-Rag complex.

Fig. S8. Analysis of the diffraction data with the Diffraction Anisotropy Server (*26*).

Table S1. Strains used in this study.

Table S2. Plasmids used in this study.

References (*34*–*38*)

REFERENCES AND NOTES

1. R. A. Saxton, D. M. Sabatini, mTOR signaling in growth, metabolism, and disease. *Cell* **168**, 960–976 (2017).
2. M. Shimobayashi, M. N. Hall, Multiple amino acid sensing inputs to mTORC1. *Cell Res.* **26**, 7–20 (2016).
3. Y. Sancak, T. R. Peterson, Y. D. Shaul, R. A. Lindquist, C. C. Thoreen, L. Bar-Peled, D. M. Sabatini, The Rag GTPases bind raptor and mediate amino acid signaling to mTORC1. *Science* **320**, 1496–1501 (2008).
4. E. Kim, P. Goraksha-Hicks, L. Li, T. P. Neufeld, K.-L. Guan, Regulation of TORC1 by Rag GTPases in nutrient response. *Nat. Cell Biol.* **10**, 935–945 (2008).
5. R. Gong, L. Li, Y. Liu, P. Wang, H. Yang, L. Wang, J. Cheng, K.-L. Guan, Y. Xu, Crystal structure of the Gtr1p-Gtr2p complex reveals new insights into the amino acid-induced TORC1 activation. *Genes Dev.* **25**, 1668–1673 (2011).
6. C. Demetriades, N. Doumpas, A. A. Teleman, Regulation of TORC1 in response to amino acid starvation via lysosomal recruitment of TSC2. *Cell* **156**, 786–799 (2014).
7. T. Zhang, R. Wang, Z. Wang, X. Wang, F. Wang, J. Ding, Structural basis for Ragulator functioning as a scaffold in membrane-anchoring of Rag GTPases and mTORC1. *Nat. Commun.* **8**, 1394 (2017).
8. R. Yonehara, S. Nada, T. Nakai, M. Nakai, A. Kitamura, A. Ogawa, H. Nakatsumi, K. I. Nakayama, S. Li, D. M. Standley, E. Yamashita, A. Nakagawa, M. Okada, Structural basis for the assembly of the Ragulator-Rag GTPase complex. *Nat. Commun.* **8**, 1625 (2017).
9. M.-Y. Su, K. L. Morris, D. J. Kim, Y. Fu, R. Lawrence, G. Stjepanovic, R. Zoncu, J. H. Hurley, Hybrid structure of the RagA/C-Ragulator mTORC1 activation complex. *Mol. Cell* **68**, 835–846.e3 (2017).
10. Z. Mu, L. Wang, W. Deng, J. Wang, G. Wu, Structural insight into the Ragulator complex which anchors mTORC1 to the lysosomal membrane. *Cell Discov.* **3**, 17049 (2017).
11. M. E. G. de Araujo, A. Naschberger, B. G. Fürnrohr, T. Stasyk, T. Dunzendorfer-Matt, S. Lechner, S. Welti, L. Kremser, G. Shivalingaiah, M. Offterdinger, H. H. Lindner, L. A. Huber, K. Scheffzek, Crystal structure of the human lysosomal mTORC1 scaffold complex and its impact on signaling. *Science* **358**, 377–381 (2017).
12. L. Bar-Peled, L. D. Schweitzer, R. Zoncu, D. M. Sabatini, Ragulator is a GEF for the Rag GTPases that signal amino acid levels to mTORC1. *Cell* **150**, 1196–1208 (2012).
13. J.-H. Jeong, K.-H. Lee, Y.-M. Kim, D.-H. Kim, B.-H. Oh, Y.-G. Kim, Crystal structure of the $Gtr1p^{GTP}$-$Gtr2p^{GDP}$ protein complex reveals large structural rearrangements triggered by GTP-to-GDP conversion. *J. Biol. Chem.* **287**, 29648–29653 (2012).
14. M. Binda, M.-P. Péli-Gulli, G. Bonfils, N. Panchaud, J. Urban, T. W. Sturgill, R. Loewith, C. De Virgilio, The Vam6 GEF controls TORC1 by activating the EGO complex. *Mol. Cell* **35**, 563–573 (2009).
15. N. Panchaud, M. P. Péli-Gulli, C. De Virgilio, SEACing the GAP that nEGOCiates TORC1 activation: Evolutionary conservation of Rag GTPase regulation. *Cell Cycle* **12**, 2948–2952 (2013).
16. G. Bonfils, M. Jaquenoud, S. Bontron, C. Ostrowicz, C. Ungermann, C. De Virgilio, Leucyl-tRNA synthetase controls TORC1 via the EGO complex. *Mol. Cell* **46**, 105–110 (2012).
17. S. Kira, Y. Kumano, H. Ukai, E. Takeda, A. Matsuura, T. Noda, Dynamic relocation of the TORC1-Gtr1/2-Ego1/2/3 complex is regulated by Gtr1 and Gtr2. *Mol. Biol. Cell* **27**, 382–396 (2016).
18. K. Powis, T. Zhang, N. Panchaud, R. Wang, C. De Virgilio, J. Ding, Crystal structure of the Ego1-Ego2-Ego3 complex and its role in promoting Rag GTPase-dependent TORC1 signaling. *Cell Res.* **25**, 1043–1059 (2015).
19. R. Hatakeyama, M.-P. Péli-Gulli, Z. Hu, M. Jaquenoud, G. M. Garcia Osuna, A. Sardu, J. Dengjel, C. De Virgilio, Spatially distinct pools of TORC1 balance protein homeostasis. *Mol. Cell* **73**, 325–338.e8 (2019).
20. S. Kira, K. Tabata, K. Shirahama-Noda, A. Nozoe, T. Yoshimori, T. Noda, Reciprocal conversion of Gtr1 and Gtr2 nucleotide-binding states by Npr2-Npr3 inactivates TORC1 and induces autophagy. *Autophagy* **10**, 1565–1578 (2014).
21. T. Zhang, M.-P. Péli-Gulli, H. Yang, C. De Virgilio, J. Ding, Ego3 functions as a homodimer to mediate the interaction between Gtr1-Gtr2 and Ego1 in the EGO complex to activate TORC1. *Structure* **20**, 2151–2160 (2012).
22. R. Nicastro, A. Sardu, N. Panchaud, C. De Virgilio, The architecture of the Rag GTPase signaling network. *Biomolecules* **7**, E48 (2017).
23. K. Shen, D. M. Sabatini, Ragulator and SLC38A9 activate the Rag GTPases through noncanonical GEF mechanisms. *Proc. Natl. Acad. Sci. U.S.A.* **115**, 9545–9550 (2018).
24. T. Sekiguchi, Y. Kamada, N. Furuno, M. Funakoshi, H. Kobayashi, Amino acid residues required for Gtr1p-Gtr2p complex formation and its interactions with the Ego1p-Ego3p complex and TORC1 components in yeast. *Genes Cells* **19**, 449–463 (2014).

25. W. Kabsch, XDS. *Acta Crystallogr.* **D66**, 125–132 (2010).
26. M. Strong, M. R. Sawaya, S. Wang, M. Phillips, D. Cascio, D. Eisenberg, Toward the structural genomics of complexes: Crystal structure of a PE/PPE protein complex from *Mycobacterium tuberculosis*. *Proc. Natl. Acad. Sci. U.S.A.* **103**, 8060–8065 (2006).
27. I. J. Tickle, C. Flensburg, P. Keller, W. Paciorek, A. Sharff, C. Vonrhein, G. Bricogne, *STARANISO* (Global Phasing Ltd., 2018).
28. P. D. Adams, P. V. Afonine, G. Bunkóczi, V. B. Chen, I. W. Davis, N. Echols, J. J. Headd, L.-W. Hung, G. J. Kapral, R. W. Grosse-Kunstleve, A. J. McCoy, N. W. Moriarty, R. Oeffner, R. J. Read, D. C. Richardson, J. S. Richardson, T. C. Terwilliger, P. H. Zwart, PHENIX: A comprehensive Python-based system for macromolecular structure solution. *Acta Crystallogr.* **D66**, 213–221 (2010).
29. G. N. Murshudov, P. Skubák, A. A. Lebedev, N. S. Pannu, R. A. Steiner, R. A. Nicholls, M. D. Winn, F. Long, A. A. Vagin, REFMAC5 for the refinement of macromolecular crystal structures. *Acta Crystallogr.* **D67**, 355–367 (2011).
30. P. Emsley, K. Cowtan, Coot: Model-building tools for molecular graphics. *Acta Crystallogr.* **D60**, 2126–2132 (2004).
31. M. D. Winn, C. C. Ballard, K. D. Cowtan, E. J. Dodson, P. Emsley, P. R. Evans, R. M. Keegan, E. B. Krissinel, A. G. W. Leslie, A. McCoy, S. J. McNicholas, G. N. Murshudov, N. S. Pannu, E. A. Potterton, H. R. Powell, R. J. Read, A. Vagin, K. S. Wilson, Overview of the CCP4 suite and current developments. *Acta Crystallogr.* **D67**, 235–242 (2011).
32. Schrödinger, LLC, The PyMOL Molecular Graphics System, Version 2.0 (Schrödinger, LLC, 2015).
33. M.-P. Péli-Gulli, A. Sardu, N. Panchaud, S. Raucci, C. De Virgilio, Amino acids stimulate TORC1 through Lst4-Lst7, a GTPase-activating protein complex for the Rag family GTPase Gtr2. *Cell Rep.* **13**, 1–7 (2015).
34. P. Gouet, E. Courcelle, D. I. Stuart, F. Métoz, ESPript: Analysis of multiple sequence alignments in PostScript. *Bioinformatics* **15**, 305–308 (1999).
35. I. Pedruzzi, F. Dubouloz, E. Cameroni, V. Wanke, J. Roosen, J. Winderickx, C. De Virgilio, TOR and PKA signaling pathways converge on the protein kinase Rim15 to control entry into G_0. *Mol. Cell* **12**, 1607–1613 (2003).
36. C. B. Brachmann, A. Davies, G. J. Cost, E. Caputo, J. Li, P. Hieter, J. D. Boeke, Designer deletion strains derived from *Saccharomyces cerevisiae* S288C: A useful set of strains and plasmids for PCR-mediated gene disruption and other applications. *Yeast* **14**, 115–132 (1998).
37. R. D. Gietz, A. Sugino, New yeast-*Escherichia coli* shuttle vectors constructed with in vitro mutagenized yeast genes lacking six-base pair restriction sites. *Gene* **74**, 527–534 (1988).
38. V. Wosika, E. Durandau, C. Varidel, D. Aymoz, M. Schmitt, S. Pelet, New families of single integration vectors and gene tagging plasmids for genetic manipulations in budding yeast. *Mol. Genet. Genomics* **291**, 2231–2240 (2016).

Acknowledgments: We thank the staff members at BL18U and BL19U1 of National Facility for Protein Science in Shanghai (NFPSS) and BL17U of Shanghai Synchrotron Radiation Facility (SSRF) for technical assistance in diffraction data collection and Y. Xu and R. Hatakeyama for plasmids. **Funding:** This research was supported by grants from the National Natural Science Foundation of China (31530013 and 31870722) to J.D. and T.Z. and the Swiss National Science Foundation (310030_166474) to C.D.V. **Author contributions:** T.Z. carried out the structural studies. M.-P.P.-G. performed the functional studies. Z.Z., X.T., and J.Y. carried out the protein expression and purification, and crystallization experiments. T.Z., M.-P.P.-G., C.D.V., and J.D. conceived the study and participated in the experimental design, data analyses, as well as discussion, writing, and editing of the manuscript. **Competing interests:** The authors declare that they have no competing interests. **Data and materials availability:** All data needed to evaluate the conclusions in the paper are present in the paper and/or the Supplementary Materials. Additional data related to this paper may be requested from the authors. The structure of the EGOC has been deposited in the RCSB PDB with accession code 6JWP.

Submitted 25 April 2019
Accepted 26 August 2019
Published 25 September 2019
10.1126/sciadv.aax8164

Citation: T. Zhang, M.-P. Péli-Gulli, Z. Zhang, X. Tang, J. Ye, C. De Virgilio, J. Ding, Structural insights into the EGO-TC–mediated membrane tethering of the TORC1-regulatory Rag GTPases. *Sci. Adv.* **5**, eaax8164 (2019).